applied sciences

MDPI

Article

Adaptive Control of Flapping-Wing Micro Aerial Vehicle with Coupled Dynamics and Unknown Model Parameters

Jiawang Mou [1,2], Weiping Zhang [1,*], Chaofeng Wu [1,2] and Qingcheng Guo [1,2]

1 National Key Laboratory of Science and Technology on Micro/Nano Fabrication, Shanghai Jiao Tong University, Shanghai 200240, China
2 Department of Micro/Nano Electronics, School of Electronic Information and Electrical Engineering, Shanghai Jiao Tong University, Shanghai 200240, China
* Correspondence: zhangwp@sjtu.edu.cn

Abstract: With the complex aerodynamics, the accurate system model of the flapping-wing micro aerial vehicle required for precise control is hard to acquire, meanwhile, due to the unique control strategy, the coupling between the actuators also brings a great challenge to the control of the vehicle. In this paper, we establish a theoretical model of the vehicle. Based on this model, we propose a multiaxial adaptive controller with the reference generator for the attitude and altitude control using the backstepping design method, the stability of this controller is proved by the Lyapunov function. Moreover, a control allocation algorithm is proposed to coordinate the different actuators such that they together produce the desired virtual control efforts. In addition, we detail the lightweight design of the flapping-wing micro aerial vehicle with altitude and attitude sensing onboard. Then, the effectiveness of the proposed control scheme is verified by the simulation and the flight test with multi-axis simultaneous control conducted on this lightweight vehicle. The experimental results show that the controller can maintain hovering flight and ensure the convergence of the adaptive parameters even when the unilateral thrust of the vehicle is not enough due to manufacturing and assembly errors. This work provides an idea for us to explore how insects maintain stable flight in the face of changes in their model parameters.

Keywords: micro aerial vehicle; flapping wing; adaptive control; decoupling control

check for updates

Citation: Mou, J.; Zhang, W.; Wu, C.; Guo, Q. Adaptive Control of Flapping-Wing Micro Aerial Vehicle with Coupled Dynamics and Unknown Model Parameters. *Appl. Sci.* **2022**, *12*, 9104. https://doi.org/10.3390/app12189104

Academic Editors: Manuel Armada and Roemi Fernandez

Received: 28 August 2022
Accepted: 7 September 2022
Published: 10 September 2022

1. Introduction

The fascination toward excellent flying skill of natural fliers has inspired the development of Flapping-wing Micro Aerial Vehicle (FMAV). Researchers have been trying to uncover the secrets behind its high-lift characteristics by analyzing the aerodynamical and flow dynamic [1–4]. With the continuous progress and development of manufacturing technology, it offers us the opportunity to design FMAV to mimic and learn from natural fliers. The research object of this paper is the tailless FMAV weighing less than 30 g. From the perspective of flight control mode, this kind of FMAV is more similar to insects in nature, and 15 g$\sim$30 g is the minimum weight range that would make it possible for the FMAV to fly for more than four minutes with the propulsion system, sensor system, battery, and some mission payloads onboard. However, due to the lack of tail, the inherent instability of the FMAV makes it more difficult to control.

As of now, some flapping wing robots capable of hovering have been designed. The first ornithopter to achieve stable hovering flight is the two-wing FMAV developed by the Defense Advanced Research Projects Agency (DARPA) [5] of the United States. The control torque is generated by adjusting the trailing edge. It realizes the stable flight and the wireless transmission of images using the onboard camera. The two-wing FMAVs with similar control mothed include the 22 g Colibri robot [6] and the 21 g KUBeetle [7–9]. Among them, KUBeetle-S [10] generates the control torque by adjusting the stroke plane. In this way, the direction of the average thrust is changed and the required control torque is generated. Moreover, there are also some direct-drive, two-wing FMAVs, such as the 20.4 g hummingbird robot [11–14] and 80 mg Robobee [15], generating the three-axis torque through wing kinematics modulation. In addition, another category is four-wing FMAV. Although the four-wing flapping robot is not as closely related to insects as the two-wing FMAV, it can utilize the clap-and-fling effect to improve aerodynamic efficiency, such as DelFly series [16–18]. Most of above FMAVs can achieve stable flight with onboard batteries, control, and attitude sensing systems, but few have more sensors on board to sense states other than posture due to weight and power constraints. Only with the help of the external motion capture system, the stable control of 3D position can be implemented [19,20]. The FMAV designed in this paper is a four-wing FMAV equipped with a laser sensor and a barometer, which can rely only on its sensors to achieve altitude and attitude control.

From the control perspective, since most FMAVs are custom designed and manufactured, assembly errors and manufacturing imperfections are unavoidable. Moreover, depending on the mission requirements, the FMAV will carry different mission payloads, such as cameras, to accomplish specific tasks sometimes. All of these will make a difference between the actual model parameters of the FMAV and the theoretical model parameters, which poses a challenge to the control of the FMAV. Thus, many scholars have tried different controllers to solve these problems. In terms of attitude stability control, the most popular controller is the PID controller. In [21], a loop shaping compensator is designed and added to the PD controller to improve the low frequency gain while sustaining the stability margin. In [22], the attitude stability is achieved by the PD controller with a reference generator. It seems that a model-free PID controller can achieve attitude stability of the most FMAV, but when the model parameters of the vehicle change, the controller whose parameters have been tuned before may not work or has a limited stability margin. To aovid this problem, many nonlinear controllers have been proposed. In [23], an adaptive controller was proposed to achieve attitude control with unknown model parameters. In [24], flying with damaged wings is achieved by a hybrid controller combined with the adaptive controller and sliding mode control. However, these adaptive controllers do not include a reference generator that will provide a reasonable trajectory of setpoint which can reduce the overshoot of the control result and faster the convergence of adaptive parameters. In our previous works [25], we have designed a model-based Active Disturbance Rejection Controller (ADRC) for altitude control of the FMAV with internal and external disturbances. It showed that the ADRC can not only reduce the influence of weight change on altitude control but also has a good ability to suppress external disturbance. The ADRC with the Extended States Observer (ESO) was also applied to maintain the stable attitude of a bird-like flapping wing robot [26] during the automatic landing. However, the flapping wing produces large-amplitude, low-frequency vibration, which will introduce a lot of noise to the state measurement, especially to the attitude state perception. Thus, the selection of ESO bandwidth needs to reach a compromise between the tracking speed and signal-to-noise ratio of the estimators, which poses a great challenge for the application of ADRC controller on attitude control of the FMAV [27,28]. In addition to the lack of accurate model information, strong-coupling dynamics between attitude axes are the other significant feature. Although the decoupling of control torque and force between each axis is taken into consideration as much as possible during the mechanism design, there still exists coupling due to the limitation of the actuators' number and the complexity of the air force. In most of the above literature, the input of each actuator was assigned as a linear addition of the relevant controllers' output [15,16]. This approach is based on the assumption that the cross-axis coupling effect is not significant near the trim condition of the hovering FMAV. Although this method is more convenient for implementation, a reasonable control allocation based on the model is needed to obtain a larger domain of controllable flights.

In this paper, we concentrate on the control of a FMAV capable of hovering with unknown or time-varying model parameters relying on onboard sensors alone, the detailed hardware scheme is presented. Additionally, an adaptive controller designed by the backstepping method and a reasonable control allocation are proposed. To reduce the overshoot of the states controlled, a Tracking Differential (TD) is included as the reference regulator. The effectiveness of the proposed controller is validated through the real flight with multi-axes motion control. The main contributions are as follows: (1) A tailless FMAV capable of hovering with the attitude and altitude control relying on onboard sensors alone is proposed, which relies on onboard sensors alone. (2) An adaptive controller combined with the reference regulator is proposed and verified by the flight tests. (3) For the four-wing FMAV controlled by tilting the flapping plane, a reasonable control allocation is proposed.

The rest of the article is organized as follows. Section 2 introduces the detailed design of the tailless FMAV and establishes the rotational and altitude model. Based on this model, we derive the control allocation. Section 3 discusses the control problem of the FMAV and designs the adaptive controller based on the backstepping method. In Section 4, the effectiveness of the proposed controller is verified by the simulation and flight test. Section 5 summarizes this work.

2. Design and Modeling

2.1. FMAV Platform

The FMAV in this paper is a kind of four-wing flapping wing robot. On either side, there is a pair of wings that is propelled by a hollow cup motor. It can effectively utilize the clap-fling mechanism, one of the high lift mechanisms of insects, to improve the thrust-to-weight ratio. So that, the FMAV can carry more airborne sensors. The FMAV weighs 29.6 g, has a wingspan of 35.2 cm and a height of 13 cm. As seen in Figure 1, each flapping-wing mechanism is rotated by a servo separately. The control torque for FMAV is generated by the tilt of the flapping plane. The pitching moment and the yawing moment are produced when the flapping plane is tilted in the same direction and the opposite direction, respectively. The differential in thrust on both sides causes the rolling moment.

To have a higher lift-weight ratio and lift-power ratio, the overall control and sensing system need to be as light and low power consumption as possible, which makes it difficult for us to buy off-the-shelf kits in the market. Therefore, we custom-designed the main autopilot board and sensor board. The main autopilot board is a 4-layer Printed Circuit Board (PCB) that only weighs 1.17 g (2.3 g when antenna and unessential terminals are installed). It includes a 32-bit Cortex-M4 MCU (STM32F446ME) operating at a frequency of up to 180 MHz, an inertial measurement unit, wireless communication circuit, power regulator circuits, two motor drivers, and SPL06 barometer. As shown in Figure 2, the whole PCB size has been shrunk to a 24 mm $\times$ 19 mm $\times$ 4 mm package through the compact wiring and the reasonable layout. The sensor board shown in Figure 1 includes a Vl53L1x laser sensor, which is located at the bottom of the FMAV and is used to measure the FMAV's altitude. The laser sensor has a relatively high repeat accuracy of 2.5 mm in the range of 0$\sim$4 m. By contrast, the relative accuracy of the barometer is only 0.5 m, but it has a wider measuring range. As a result, a sensor fusion of a laser sensor and a barometer for altitude measurement will complement each other. The sensor board only weighs 169 mg, it sizes are 17 mm $\times$ 7 mm. With this lightweight control and sensing system, it is possible to implement more functionality.

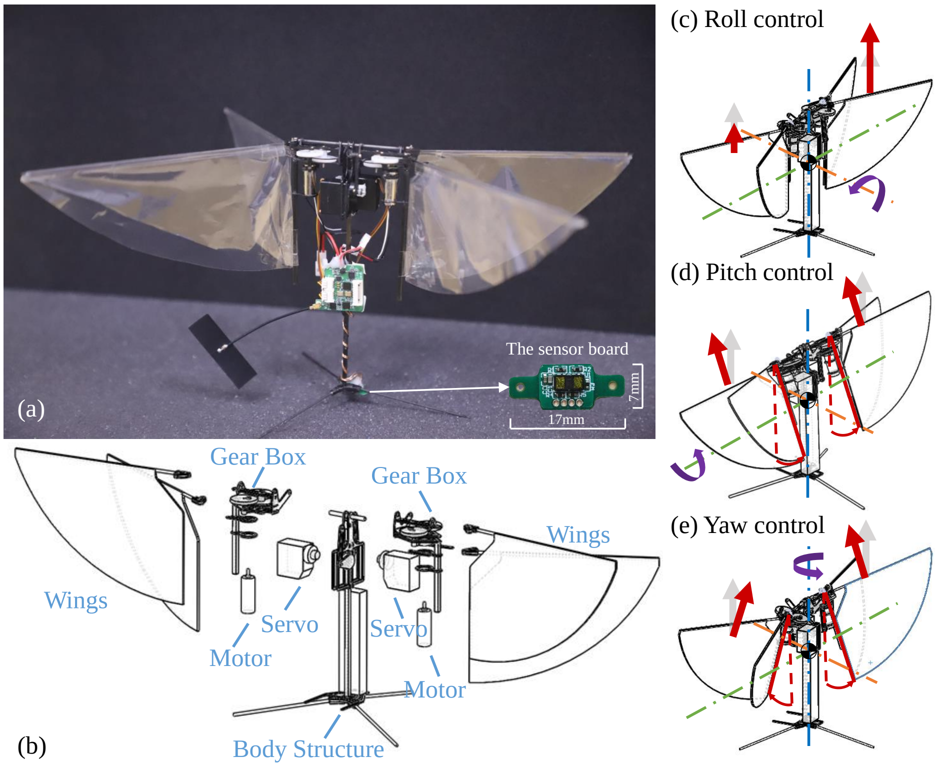

Figure 1. (**a**) Illustration of the lightweight FMAV. (**b**) Explosion diagram of mechanical structure. (**c**–**e**) Schematic diagram of control torque generation. Translucent arrows show the nominal wingbeat-average thrust vectors before torque generating. Solid arrows show wingbeat-average thrust and torque after torque generating.

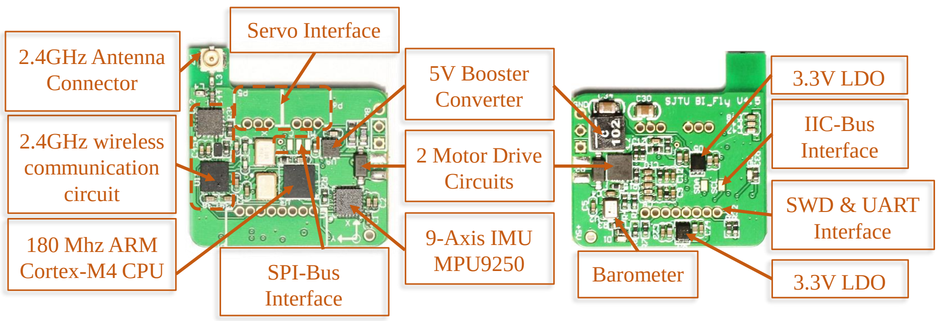

Figure 2. Illustration of the main autopilot board.

2.2. *Modeling and the Control Allocation*

To assist the controller design, we establish the dynamics model of the FMAV. Since the inertia of the wings is small relative to the inertia of the body, we assume that the FMAV is a rigid body and ignore the change in the body's moment of inertia when the wings flap. The coordinate $O^eX^eY^eZ^e$ defined in Figure 3 is the inertial coordinates. In the body coordinates $O^bX^bY^bZ^b$ fixed at the Center of Mass (CoM) of the FMAV, the rotation direction of the roll, pitch, and yaw angle is assumed to be clockwise about the X^b, Y^b, and Z^b-axis, respectively. $O^sX^sY^sZ^s$ is the flapping-plane coordinates fixed at the intersection of the fuselage and the rotation axis (Y^b-axis of the body coordinates) of the flapping wing mechanism, the Y^s-axis of the flapping-plane coordinates is parallel to the Y^b-axis, and the Z^s-axis is parallel to the trailing edge of the wing. Due to the symmetry of the body, the inertia matrix J of the FMAV can be assumed to be a diagonal matrix. The main diagonal of the inertia matrix J can be measured using the Bifilar torsional method [29].

In this paper, the dynamic model of FMAV is divided into the translational model and the rotational model as follows in Equation (1):

$$\begin{aligned} m\ddot{\boldsymbol{p}} &= \boldsymbol{F}_T - m\boldsymbol{g} \\ \boldsymbol{J}\dot{\boldsymbol{\omega}} &= \boldsymbol{\tau} + \boldsymbol{\tau}_0 - \boldsymbol{\omega} \times \boldsymbol{J}\boldsymbol{\omega} \end{aligned} \tag{1}$$

where, $\boldsymbol{\omega}$ is the angular velocity of the body, $\boldsymbol{\tau}$ represents the torque generated by the flapping wings. $\boldsymbol{\tau}_0$ represents the initial offset torque. m is the mass of the FMAV, $\boldsymbol{p} = [x, y, z]^{\mathrm{T}}$ represents the position of FMAV in the inertial coordinates. $\boldsymbol{F}_T$ represents the periodic average thrust vector in the inertial coordinates, which acts on the Center of Pressure (Cop) of the wing. $\boldsymbol{F}_T$ can be obtained by

$$\begin{aligned} \boldsymbol{F}_T &= \boldsymbol{R}_b(\boldsymbol{R}_{sl}\boldsymbol{T}_l + \boldsymbol{R}_{sr}\boldsymbol{T}_r) \\ &= \boldsymbol{R}_b\left(\begin{bmatrix} \cos\beta_l & 0 & \sin\beta_l \\ 0 & 1 & 0 \\ -\sin\beta_l & 0 & \cos\beta_l \end{bmatrix}\begin{bmatrix} 0 \\ 0 \\ f_l \end{bmatrix} + \begin{bmatrix} \cos\beta_r & 0 & \sin\beta_r \\ 0 & 1 & 0 \\ -\sin\beta_r & 0 & \cos\beta_r \end{bmatrix}\begin{bmatrix} 0 \\ 0 \\ f_r \end{bmatrix}\right) \end{aligned} \tag{2}$$

where $\boldsymbol{R}_b$ is the rotation matrix from the body coordinates to the inertial coordinates, $\boldsymbol{R}_{sl}$ and $\boldsymbol{R}_{sr}$ are the rotation matrix from the left and right flapping-plane coordinates to the body coordinates, respectively. β_l and β_r are the rotation angle of the left and right flapping planes, respectively. f_l and f_r are the scalar thrust generated by the left and right flapping wings, respectively. Expanding Equation (2), we can get the vertical component F_{Tz} of the $\boldsymbol{F}_T$:

$$\boldsymbol{F}_T = \begin{bmatrix} \cos\phi\cos\theta & -\sin\theta & \cos\phi\cos\theta & -\sin\theta \end{bmatrix}\begin{bmatrix} f_l\cos\beta_l \\ f_l\sin\beta_l \\ f_r\cos\beta_r \\ f_r\sin\beta_r \end{bmatrix} \tag{3}$$

where, ϕ and θ are the roll and pitch angle, respectively. The $\boldsymbol{\tau}$ in Equation (1) is defined by

$$\boldsymbol{\tau} = \boldsymbol{L}_{copl} \times \boldsymbol{R}_{sl}\boldsymbol{T}_l + \boldsymbol{L}_{copr} \times \boldsymbol{R}_{sr}\boldsymbol{T}_r \tag{4}$$

where, $\boldsymbol{L}_{copl}$ and $\boldsymbol{L}_{copr}$ are the vector of the CoP of the left and right wing in the body coordinates, respectively. When the flapping plane driven by the servo is tilted, the coordinates of the Cop also change accordingly. As shown in Figure 3, take for example the flapping wing mechanism on the left side, the coordinates of the Cop can be obtained by:

$$\boldsymbol{L}_{copl} = \boldsymbol{R}_s\begin{bmatrix} 0 \\ l_y \\ l_z \end{bmatrix} + \begin{bmatrix} 0 \\ 0 \\ d \end{bmatrix} \tag{5}$$

Since the two wings on one side beat symmetrically about the X^sZ^s-plane, the coordinates of the Cop can be assumed to be $[0, l_y, l_z]^{\mathrm{T}}$ in flapping-plane coordinates. The actual value of the l_y and l_z can be obtained from the relationship between force and torque in the force and torque test. d is the distance between the CoM and the point O_s. Combining Equation (4), Equation (5), and Equation (3), we can obtain the control allocation as:

$$\begin{bmatrix} \tau_x \\ \tau_y \\ \tau_z \\ \boldsymbol{F}_{Tz} \end{bmatrix} = \boldsymbol{C}\boldsymbol{U} \tag{6}$$

where,

$$
\begin{aligned}
\boldsymbol{C} &= \begin{bmatrix} l_y & 0 & -l_y & 0 \\ 0 & d & 0 & d \\ 0 & -l_y & 0 & l_y \\ \cos\phi\cos\theta & -\sin\theta & \cos\phi\cos\theta & -\sin\theta \end{bmatrix} \\
\boldsymbol{U} &= \begin{bmatrix} f_l\cos\beta_l \\ f_l\sin\beta_l \\ f_r\cos\beta_r \\ f_r\sin\beta_r \end{bmatrix} = \begin{bmatrix} U_1 \\ U_2 \\ U_3 \\ U_4 \end{bmatrix}
\end{aligned}
\tag{7}
$$

According to the above Equation, we can get the relationship between the virtual control effort U and the thrust f, the rotation angle β of the flapping plane, as shown in Equation (10).

$$
\begin{bmatrix} f_l \\ f_r \\ \beta_l \\ \beta_r \end{bmatrix} = \begin{bmatrix} \sqrt{U_1^2+U_2^2} \\ \sqrt{U_3^2+U_4^2} \\ \arctan\frac{U_2}{U_1} \\ \arctan\frac{U_4}{U_3} \end{bmatrix}
\tag{8}
$$

So far, based on this control allocation, we obtain the map from the desired force and torque to the output of actuators, using Equations (6), (7) and (10). If the actuator model describing the input-output relationship of the actuator is known, we can solve the input of the actuator according to the required force and torque outputted by the controller.

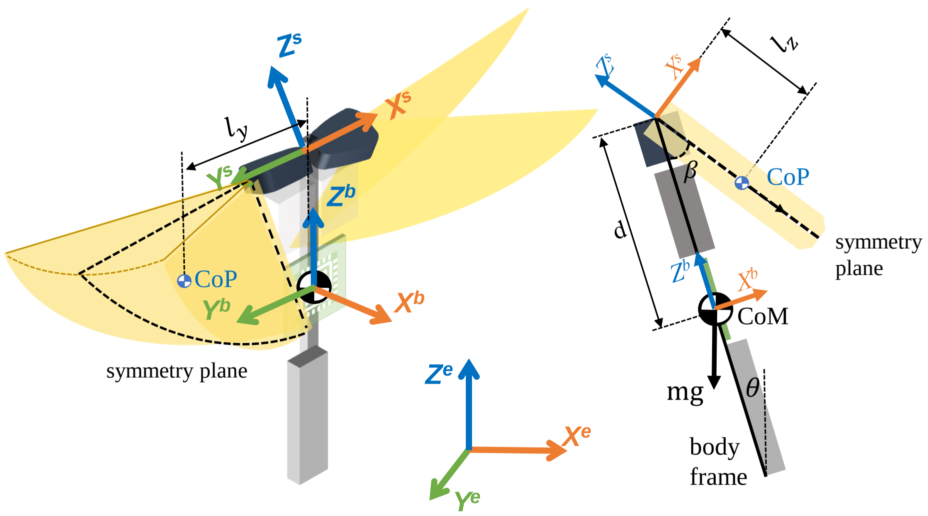

Figure 3. Illustration of model parameters and coordinates.

However, the actual actuator model contains the lift forces and torque as functions of instantaneous wing motion, which is very complex. Considering that the wings flap quickly and with a periodic nature, we make an assumption that the instantaneous lift forces on the rigid body are approximated by wing stroke average forces. In this scenario, We can obtain the actuator model by measuring the average force and torque under different actuator inputs. A 6-axis force/torque test platform (Nano17Ti, ATI) is set up as illustrated in Figure 4. The actuator model is divided into the thrust model and the servo model. The thrust model describes the relationship between the input of the motor and the magnitude of the thrust generated by the wings. The servo model describes the relationship between the input of the servo and the rotation angle of the flapping plane. The input of the motor and servo is the Pulse-Width Modulation (PWM) signal with a variable duty cycle. To obtain the thrust model, the position of the servo is fixed in the middle position, with the different control inputs of the motor, and the thrust is measured. For the servo model, under the condition of fixed motor input, with the different control input of the servo, we measure the average thrust on three axes, hence the rotation angle of the thrust can be obtained to get the relationship between the servo input and rotation angle of the flapping plane. The measured data and fitting results of the actuator model are shown in Figure 5.

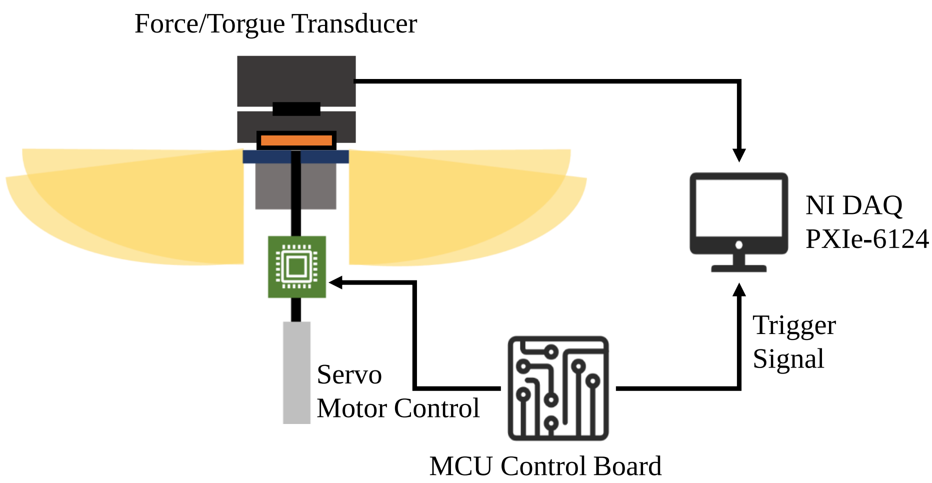

Figure 4. Illustration of force and torque test.

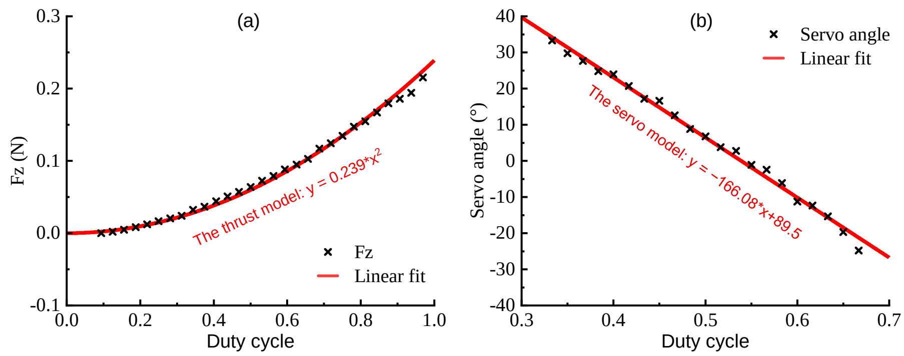

Figure 5. The actuator model. (**a**) The thrust model. (**b**) The servo model.

All of the goodness of fits are more than 0.99. So the actuator model can be expressed as

$$\begin{cases} f = 0.239u^2 \\ \beta = -166.08u_s + 89.5 \end{cases} \tag{9}$$

Here, u, u_s are the duty cycle as the input to the motor and servo respectively, the range is 0∼1. f represents the thrust in scalar form the unit is N. β is the rotation angle of the flapping-wing plane.

In summary, we establish the rotational and altitude model of the FMAV and the actuator model. If the required torque and thrust are given, we can solve for the input of the motors and servos, using Equations (6)–(9). The physical model parameters of the FMAV reported in this paper are shown in Table 1:

Table 1. Parameters of the FMAV's dynamic model.

Term	Definition	Value	Unit
J_{xx}	the moment of inertia about the X axis	364	g·cm^2
J_{yy}	the moment of inertia about the Y axis	294	g·cm^2
J_{zz}	the moment of inertia about the Z axis	343	g·cm^2
d	the distance between the point O and the CoM	6	cm
$[0, l_y, l_z]$	the coordinates of the Cop (left) in the flapping plane coordinates	$[0, 7.289, 4.5]$	cm
m	vehicle mass	29.6	g

3. Flight Control

In this section, to address the control issue caused by the discrepancy between the practical model and theoretical model, such as thrust imbalance generated during the processing and manufacturing of FMAV, we propose an adaptive controller designed by the backstepping method to estimate unknown model parameters, which includes an attitude controller and an altitude controller. The main goal of these controllers is to ensure that the FMAV can track the desired trajectory of the attitude and altitude simultaneously, even if the parameters of the practical model are different due to different prototypes or having the slow time-varying model parameters during flight, the vehicle can maintain stable flight and have high control accuracy. The block diagram representing this controller is presented in Figure 6. Its stability is proved by the Lyapunov stability theorem.

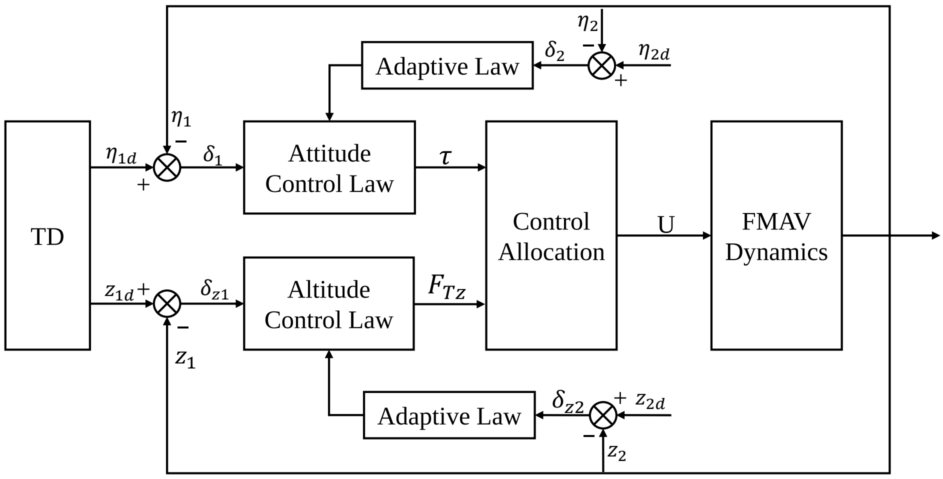

Figure 6. The block diagram of the attitude and altitude controller.

3.1. Tracking Differentiator (TD)

Since the input commands are usually abrupt, resulting in a large and persistent error before the state catch up with the command. If there is a differential term in the controller, this abrupt change will often cause saturation of the controller output, so that the system overshoot occurs with high probability. Therefore, a reasonable transient trajectory of the command that the system can follow is needed. This paper adopts the TD proposed by [27], TD's discrete form is as follows:

$$\begin{cases} \dot{v}_1(t) = v_2(t) \\ \dot{v}_2(t) = \mathrm{fhan}(v_1 - v, v_2, r, N_0 h) \end{cases} \tag{10}$$

where v is the command as the input of TD, v_1 is the desired trajectory, v_2 is the derivative of v_1. N_0 is the filter factor of TD, which can be tuned according to the smoothness of convergence, h is the sampling period. $\mathrm{fhan}(x_1, x_2, r, h)$ is a time-optimal solution in discrete form that guarantees the fastest convergence from the desired trajectory v_1 to the command v. The expression of this function can be found in [27]. r is a key parameter, equivalent to the maximum acceleration of the transient trajectory, which directly determines the speed of convergence. In this controller, each control channel has a TD, which outputs a reasonable desired value according to the input command.

3.2. Attitude Controller

Stable attitude control is the essential precondition for position control. From Equation (1), the attitude dynamics can be described by the following equation:

$$\begin{cases} \dot{\boldsymbol{\eta}}_1 = \boldsymbol{\eta}_2 \\ \dot{\boldsymbol{\eta}}_2 = \boldsymbol{J}^{-1}(\boldsymbol{\tau} + \boldsymbol{\tau_0} - \boldsymbol{\omega} \times \boldsymbol{J}\boldsymbol{\omega}) \end{cases} \tag{11}$$

where, we define the attitude angle of the vehicle as $\boldsymbol{\eta} = [\phi, \theta, \psi]^T$. ϕ, θ, and ψ are defined as the roll, pitch, and yaw angle, respectively. Then $\boldsymbol{\eta}_2 = \left[\dot{\phi}, \dot{\theta}, \dot{\psi}\right]^T$ are define as the angular velocity of the vehicle. The tracking error associated with the dynamics of the FMAV can be represented by

$$\begin{aligned} \delta_1 &= \boldsymbol{\eta}_{1d} - \boldsymbol{\eta}_1 \\ \delta_2 &= \boldsymbol{\eta}_{2d} - \boldsymbol{\eta}_2 \end{aligned} \tag{12}$$

where, $\boldsymbol{\eta}_{2d}$ is the desired angular velocity of the FMAV. Let us consider the candidate Lyapunov function $\boldsymbol{V}_1$ as follow:

$$V_1 = \frac{1}{2}\boldsymbol{\delta_1}^T \boldsymbol{A_1} \boldsymbol{\delta_1} \tag{13}$$

where $\boldsymbol{A_1} \in \boldsymbol{R}^{3\times3}$ is a positive diagonal matrix, and the derivative of this Lyapunov function $\dot{\boldsymbol{V}}_1$ is defined by

$$\dot{V}_1 = \boldsymbol{\delta_1}^T \boldsymbol{A_1} \dot{\boldsymbol{\delta}}_\mathbf{1} = \delta_1^T \boldsymbol{A_1}(\dot{\boldsymbol{\eta}}_{1d} - \dot{\boldsymbol{\eta}}_1) = \delta_1^T \boldsymbol{A}_1(\dot{\boldsymbol{\eta}}_{1d} - \boldsymbol{\eta}_2) \tag{14}$$

We define the desired angular velocity $\boldsymbol{\eta}_{2d}$ as:

$$\boldsymbol{\eta}_{2d} = \dot{\boldsymbol{\eta}}_{1d} + \boldsymbol{A}_2 \delta_1 \tag{15}$$

where $\boldsymbol{A_2} \in \boldsymbol{R}^{3\times3}$ is a positive diagonal matrix. If the angular velocity $\boldsymbol{\eta}_2$ equals the desired angular velocity $\boldsymbol{\eta}_{2d}$, the $\dot{\boldsymbol{V}}_1$ in Equation (14) can be rewritten as follows:

$$\dot{V}_1 = -\delta_1^T \boldsymbol{A_1} \delta_1 < 0, \forall \delta_1 \neq 0 \tag{16}$$

According to the Invariant set theorem, the derivative of the Lyapunov function $\dot{\boldsymbol{V}}_1$ is negative. That is to say, δ_1 will converge to 0 asymptotically.

In attitude control, we take the body's moment of inertia and bias torque as adaptive estimators. Then, the candidate Lyapunov function $\boldsymbol{V}_2$ is designed as follows:

$$V_2 = \frac{1}{2}\delta_1^T \boldsymbol{A}_1 \delta_1 + \frac{1}{2}\delta_2^T \boldsymbol{J} \delta_2 + \frac{1}{2}\tilde{\boldsymbol{\alpha}}^T \boldsymbol{\Gamma} \tilde{\boldsymbol{\alpha}} \tag{17}$$

where, $\boldsymbol{J}$ is the actual inertia matrix. The adaptive model parameter is defined as $\hat{\boldsymbol{\alpha}} = \begin{bmatrix} \hat{J}_{xx} & \hat{J}_{yy} & \hat{J}_{zz} & \hat{\tau}_{0x} & \hat{\tau}_{0y} & \hat{\tau}_{0z} \end{bmatrix}^{\mathrm{T}}$. $\hat{J}_{xx}$, $\hat{J}_{yy}$, and $\hat{J}_{zz}$ are the components of the estimated moment of inertia in the x, y, and z-axis, respectively. $\hat{\tau}_{0x}$, $\hat{\tau}_{0y}$, and $\hat{\tau}_{0z}$ are the components of the estimated bias torque in the x, y, and z-axis directions, respectively. $\tilde{\boldsymbol{\alpha}}$ is the estimation error defined as $\tilde{\boldsymbol{\alpha}} = \boldsymbol{\alpha} - \hat{\boldsymbol{\alpha}}$. $\boldsymbol{\Gamma}$ is a positive diagonal gain matrix. Thus, the derivative of this Lyapunov function $\dot{\boldsymbol{V}}_2$ is defined by:

$$\begin{aligned}\dot{V}_2 &= \boldsymbol{\delta}_1^T \boldsymbol{A}_1 \dot{\boldsymbol{\delta}}_1 + \boldsymbol{\delta}_2^T \boldsymbol{J} \dot{\boldsymbol{\delta}}_2 + \tilde{\boldsymbol{\alpha}}^T \boldsymbol{\Gamma} \dot{\tilde{\boldsymbol{\alpha}}} \\ &= \boldsymbol{\delta}_1^T \boldsymbol{A}_1 (\dot{\boldsymbol{\eta}}_{1d} - (\boldsymbol{\eta}_{2d} - \boldsymbol{\delta}_2)) + \boldsymbol{\delta}_2^T \boldsymbol{J} \dot{\boldsymbol{\delta}}_2 + \tilde{\boldsymbol{\alpha}}^T \boldsymbol{\Gamma} \dot{\tilde{\boldsymbol{\alpha}}} \\ &= -\boldsymbol{\delta}_1^T \boldsymbol{A}_1 \boldsymbol{A}_2 \boldsymbol{\delta}_1 + \boldsymbol{\delta}_2^T (\boldsymbol{A}_1 \boldsymbol{\delta}_1 + \boldsymbol{J}(\dot{\boldsymbol{\eta}}_{2d} - \dot{\boldsymbol{\eta}}_2)) + \tilde{\boldsymbol{\alpha}}^T \boldsymbol{\Gamma} \dot{\tilde{\boldsymbol{\alpha}}}\end{aligned} \tag{18}$$

Substituting Equation (11) into Equation (18), Equation (18) can be rewritten as

$$\dot{V}_2 = -\boldsymbol{\delta}_1^T \boldsymbol{A}_1 \boldsymbol{A}_2 \boldsymbol{\delta}_1 + \boldsymbol{\delta}_2^T (\boldsymbol{A}_1 \boldsymbol{\delta}_1 + \boldsymbol{J} \dot{\boldsymbol{\eta}}_{2d} - (\boldsymbol{\tau} + \boldsymbol{\tau}_0 - \boldsymbol{\omega} \times \boldsymbol{J} \boldsymbol{\omega})) + \tilde{\boldsymbol{\alpha}}^T \boldsymbol{\Gamma} \dot{\tilde{\alpha}} \tag{19}$$

To make this system asymptotically stable, we design the control law as:

$$\begin{aligned}\boldsymbol{\tau} &= \boldsymbol{A}_1 \boldsymbol{\delta}_1 + \boldsymbol{A}_3 \boldsymbol{\delta}_2 + \hat{\boldsymbol{J}} \dot{\boldsymbol{\eta}}_{2d} - \hat{\boldsymbol{\tau}}_0 + \boldsymbol{\omega} \times \boldsymbol{J} \boldsymbol{\omega} \\ &= \boldsymbol{A}_1 \boldsymbol{\delta}_1 + \boldsymbol{A}_3 \boldsymbol{\delta}_2 + \boldsymbol{Y} \hat{\boldsymbol{\alpha}}\end{aligned} \tag{20}$$

where $\boldsymbol{A_3} \in \boldsymbol{R}^{3\times 3}$ is a positive diagonal gain matrix, and the matrix $\boldsymbol{Y}$ is:

$$\boldsymbol{Y} = \begin{bmatrix} \dot{\eta}_{2dx} & -\omega_y \omega_z & \omega_y \omega_z & 1 & 0 & 0 \\ \omega_x \omega_z & \dot{\eta}_{2dy} & -\omega_x \omega_z & 0 & 1 & 0 \\ -\omega_x \omega_y & \omega_x \omega_y & \dot{\eta}_{2dz} & 0 & 0 & 1 \end{bmatrix} \tag{21}$$

Then, Equation (19) becomes

$$\dot{V}_2 = -\boldsymbol{\delta}_1^T \boldsymbol{A}_1 \boldsymbol{A}_2 \boldsymbol{\delta}_1 - \boldsymbol{\delta}_2^T \boldsymbol{A}_3 \boldsymbol{\delta}_2 + \tilde{\boldsymbol{\alpha}}^T \left(\boldsymbol{\Gamma} \dot{\tilde{\boldsymbol{\alpha}}} + \boldsymbol{Y}^T \boldsymbol{\delta}_2 \right) \tag{22}$$

So we can design the adaptive law as

$$\dot{\tilde{\boldsymbol{\alpha}}} = -\boldsymbol{\Gamma}^{-1} \boldsymbol{Y}^T \boldsymbol{\delta}_2 \tag{23}$$

Thus, the derivative of the Lyapunov function $\dot{V}_2$ is negative. According to the Invariant set theorem, the system will be asymptotically stable. That is to say, the tracking error $\boldsymbol{\delta}_1$ and the estimation error of the model parameters $\hat{\boldsymbol{\alpha}}$ will converge to 0, and the state of FMAV can track the command value. This designed controller can not only stabilize the system through the state feedback control loop but also adapt the parameters of the model in real-time according to the state error.

3.3. Altitude Controller

The altitude controller is similar to the attitude controller and is designed according to the dynamic model as shown in Equation (1).

$$\begin{cases} \dot{z}_1 = z_2 \\ m\dot{z}_2 = F_{zT} - mg \end{cases} \tag{24}$$

where z_1 and z_2 are the altitude and vertical velocity of the FMAV, respectively. Different from attitude control, the altitude controller chooses the vehicle mass estimator $\hat{m}$ as an adaptive parameter to account for misalignment between the theoretical and practical thrust model or the change in the vehicle's weight. The difference between the mass estimator $\hat{m}$ and the practical mass m is defined as the adaptive parameter error $\tilde{m} = m - \hat{m}$. Similar to the attitude controller design, the altitude error δ_{z1} and the vertical velocity error δ_{z2} associated with the altitude dynamics of the FMAV is defined by:

$$\begin{aligned}\delta_{z1} &= z_{1d} - z_1 \\ \delta_{z2} &= z_{2d} - z_2\end{aligned} \tag{25}$$

where, z_{1d} and z_{2d} are the desired altitude and vertical velocity of the FMAV, respectively. Then, we define the Lyapunov function V_{z1}, V_{z2} as

$$\begin{cases} V_{z1} = \frac{1}{2}K_1\delta_{z1}^2 \\ V_{z2} = \frac{1}{2}K_1\delta_{z1}^2 + \frac{1}{2}m\delta_{z2}^2 + \frac{1}{2}\Gamma_z\tilde{m}^2 \end{cases} \tag{26}$$

So we can get the time derivative of the Lyapunov function $\dot{V}_{z1}$, $\dot{V}_{z2}$ as follow:

$$\begin{cases} \dot{V}_{z1} = K_1\delta_{z1}\dot{\delta}_{z1} = K_1\delta_{z1}(\dot{z}_{1d} - z_2) \\ \dot{V}_{z2} = \dot{V}_{z1} + m\delta_{z2}\dot{\delta}_{z2} + K_3\tilde{m}\dot{\tilde{m}} \\ \quad\;\; = \dot{V}_{z1} + \delta_{z2}(m\dot{z}_{2d} - (F_{zT} - mg)) + \Gamma_z\tilde{m}\dot{\tilde{m}} \end{cases} \tag{27}$$

We propose the control law as

$$\begin{aligned} z_{2d} &= \dot{z}_{1d} + K_2\delta_{z1} \\ F_{zT} &= K_1\delta_{z1} + \hat{m}\dot{z}_{2d} + \hat{m}g + K_3\delta_{z2} \end{aligned} \tag{28}$$

As a result, Equation (27) becomes

$$\begin{cases} \dot{V}_{z1} = K_1\delta_{z1}(-K_2\delta_{z1} + \delta_{z2}) \\ \dot{V}_{z2} = -K_1K_2\delta_{z1}^2 - K_3\delta_{z2}^2 + \delta_{z2}\tilde{m}(\dot{z}_{2d} + g) + \Gamma_z\tilde{m}\dot{\tilde{m}} \end{cases} \tag{29}$$

To make the system asymptotically stable, we derive the adaptive law as:

$$\dot{\tilde{m}} = -\Gamma_z^{-1}\delta_{z2}(\dot{z}_{2d} + g) \tag{30}$$

In this way, Equation (29) can be rewritten as

$$\dot{V}_{z2} = -K_1K_2\delta_{z1}^2 - K_3\delta_{z2}^2 \le 0 \tag{31}$$

which renders the derivative of the Lyapunov function V_{z1} and V_{z2} to be negative define. According to the Invariant set theorem, the altitude control will be asymptotically stable. the height error δ_{z1} will converge to 0. That is, the altitude state of the vehicle can follow the altitude command.

4. Experiment and Discussion

In this section, we conduct digital simulations and the real flight experiment to verify the effectiveness of the controller. The purpose of the simulation is twofold: (1) to evaluate the control effect of the proposed controller when the time-varying control command is input; (2) to compare the control effect of the proposed adaptive controller and the PID controller. In addition, a real flight test is implemented on the real FMAV with thrust attenuation on one side. The magnitude of thrust attenuation is unknown before the experiment, and this flight experiment is used to evaluate the control effect of the proposed controller in the presence of uncertain model parameters. The tracking performance in simulation and flight is evaluated based on the Root-Mean-Square (RMS) errors of tracked state, system overshoot, and decoupling performance.

4.1. Simulation

The simulation is carried out in Simulink. To make the simulation model closer to the practical model, the air damping model is added, and the specific modeling method and parameters can be found in [30,31]. The parameters presented in Table 1 are chosen as the model parameters of the FMAV. To explore whether the designed controller has a large enough control domain and good decoupling performance, we take different types of time-varying control commands, including step command, sinusoidal command, constantvalued command, and triangular waveform command, as the inputs to different axes, simultaneously. Specific commands are shown as follows:

$$\begin{aligned}
\phi_d &= 20 \times \text{square}(\pi t) \\
\theta_d &= 10 \\
\psi_d &= 20 \times \sin(\pi t/2) \\
z_d &= \begin{cases} 100, & 0s < t < 5\ \text{s} \\ 100 + 20 \times \text{sawtooth}(2\pi t/15, 0.5), & t \geq 5\ \text{s} \end{cases}
\end{aligned} \tag{32}$$

where, ϕ_d, θ_d, ψ_d, and z_d are the reference of the roll, pitch, yaw angle, and altitude, respectively. The Matlab function square() and sawtooth() generate the square waves and triangular waveform, respectively. In the simulation, these commands are input to the vehicle simultaneously. The initial state of the attitude and altitude of the FMAV are both 0. The ideal outcome of the control task is to enable all states to track the reference without errors and overshooting. For comparison, we also design a cascade PID controller in simulation for the identical task. This kind of cascade PID controller is commonly applied in the quadrotor. The inner loop is the angular velocity or vertical velocity loop, and the outer loop is the angle or altitude loop. Simple linear control allocation shown in Equation (33) is adopted.

$$\begin{cases} PWM_{fl} = O_{thrust} - O_{roll} \\ PWM_{fr} = O_{thrust} + O_{roll} \\ PWM_{sl} = -O_{pitch} - O_{yaw} \\ PWM_{sr} = O_{pitch} - O_{yaw} \end{cases} \tag{33}$$

where, PWM_{fl} and PWM_{fr} are the control inputs of the left and right motors, respectively. PWM_{sl} and PWM_{sr} are the control inputs of the left and right servos, respectively. O_{roll}, O_{pitch}, O_{yaw} are the output of the PID controller in the roll, pitch, and yaw axis, respectively. O_{thrust} is the output of the altitude controller. This kind of control allocation is simple and more intuitive, but it ignores the coupling dynamics between every axis. Simulation results of the PID controller are shown in Figure 7.

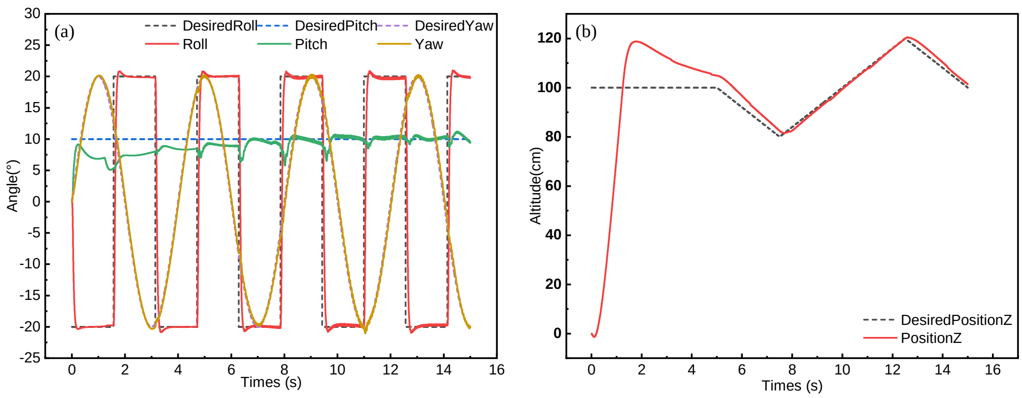

Figure 7. Simulation results of the attitude and altitude controlled by the PID controller. (**a**) Simulation results of attitude control. (**b**) Simulation results of altitude control.

As can be seen from Figure 7, all the states can converge to the desired value. However, the coupling phenomenon among the three attitude axes is obvious. when the reference of roll angle is suddenly changed, an abrupt change occurs in the pitch angle, resulting in a big error in pitch angle. In my opinion, the main reason for this phenomenon is that the interaction between the actuator outputs is not considered. When the reference of the roll angle changes, the output of the roll-axis controller changes the thrust of the wings on both sides, and the new output of the actuators cannot produce the required pitch-axis torque, resulting in a large error in the pitch angle under the influence of wind resistance. Moreover, the roll angle control and altitude control have obvious overshoot, which is caused by the integral term in the PID controller accumulating the significant error during the rising process. The maximum overshoot in altitude control is 20%. However, the integral term is also essential to eliminate the steady-state error, especially in the case of persistent wind disturbance. Compared with the PID controller, the simulation result of the proposed adaptive controller is shown in Figure 8.

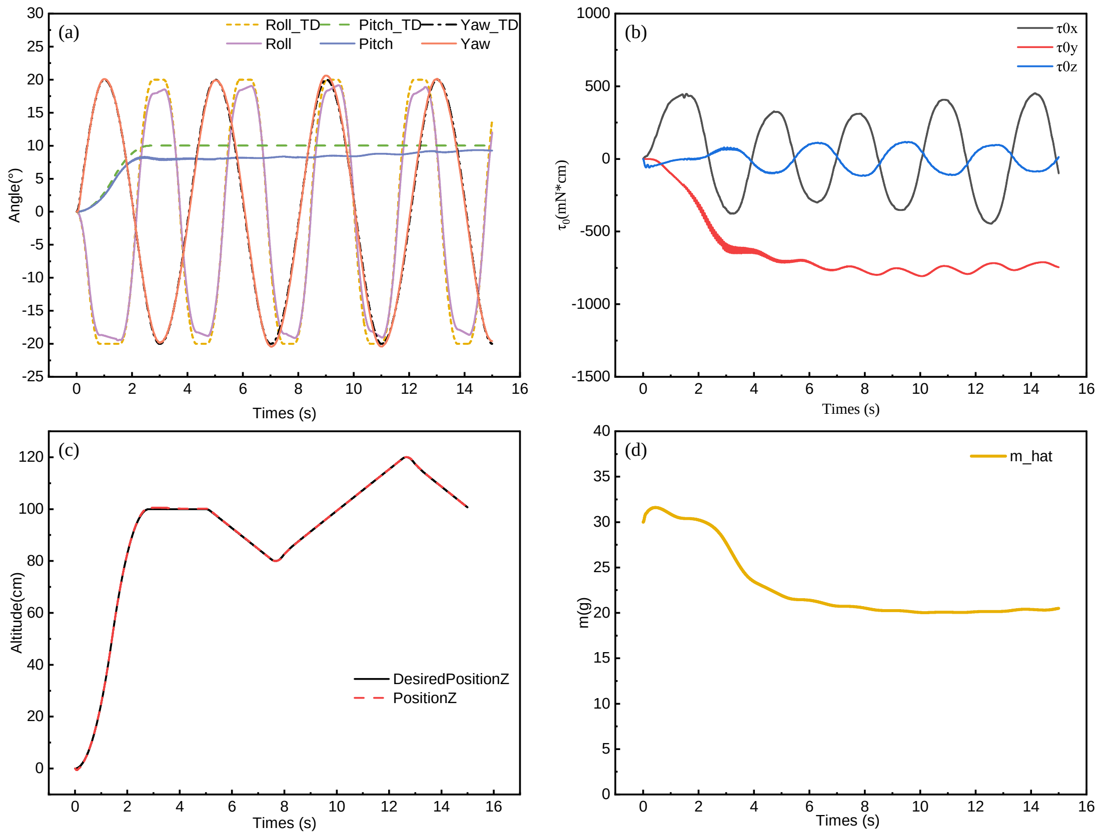

Figure 8. Simulation results of the adaptive attitude and altitude controller. The dashed lines are the control references. (**a**) Simulation results of attitude control. (**b**) The adaptation of bias torque. (**c**) Simulation results of altitude control. (**d**) The adaptation of mass.

As can be seen from Figure 8a, all states of the FMAV can well track the reference output by the TD. Thanks to the proper state trajectory planning generated by the TD, there is almost no overshoot in the control of any states even when the reference of roll angle is a rectangular wave changing back and forth. At the same time, no obvious coupling phenomenon is observed. As shown in Figure 8b, the adaptive parameters fluctuate frequently, because both positive and negative changes in attitude will cause the vehicle's velocity to change back and forth. As a result, the air resistance the FMAV encounters will also change positively and negatively, causing a fluctuation in the bias torque's adaptation. It can be inferred that the adaptive process of parameters can well reflect the variation trend of the bias torque.

Since the references of the states change constantly, the RMS error of the attitude over the entire process is considered as the index to quantify the control accuracy. For altitude control, since there is a big gap between the desired altitude and the altitude in the initial state, the RMS error will be calculated when the height is close to the set value, that is, 5 s after taking off. The RMS state errors with both controllers are listed in Table 2. Obviously, the RMS error of the adaptive controller in all axes is smaller than that of the PID controller.

It can be concluded that the adaptive controller is significantly better than the PID controller in tracking performance.

Table 2. Comparison of the RMS attitude and altitude errors from the adaptive controller and the PID controller.

Controller	RMS Error			
	Roll (°)	Pitch (°)	Yaw (°)	Altitude (cm)
Adaptive controller	1.363	1.484	0.352	0.171
PID controller	6.752	1.726	0.635	2.483

4.2. Flight Test

The proposed controller is also tested on the FMAV shown in Figure 1. The embedded software is completely developed by us based on the FreeRTOS platform. Since the vehicles are manually assembled, the consistency of the thrust model on both sides of each prototype cannot be completely guaranteed. As the number of flights and the severity of wear increases, the thrust model shows time-varying characteristics. In this flight test, we carried out the hovering flight test indoors. According to the previous flight experience, the vehicle in this flight has unilateral thrust deficiency, which was also verified in the subsequent flight data. The FMAV maintained a stable flight at an altitude of 160 cm after autonomous take-off. Meanwhile, the desired values of roll angle and yaw angle were set by random operation of the remote control stick. The difference is that the desired roll angle is directly determined by the position of the rocker, but the position of the rocker corresponding to the yaw axis determines the desired yaw rate. The flight results are as follows:

As shown in Figure 9a, on account of the obvious difference in thrust between the left and right sides, the roll angle is always less than the reference value after the FMAV takes off. It can be inferred that the thrust of the left side is smaller than that of the right side, and the vehicle has an bias torque with a negative sign. This is also consistent with the convergence trend of roll axis torque shown in Figure 9b. The adaptive parameters converge to a relatively stable value in about 25 seconds. To reflect the change of control accuracy before and after the convergence of the adaptive parameters, we calculate the RMS of the attitude error respectively, and the results are shown in Figure 10.

We can see that the RMS roll angular error is reduced by 44%, and the RMS yaw angular error is reduced by 15% after the convergence of the adaptive parameters. It can conclude that the adaptive controller can improve the control accuracy and eliminate steady-state error. For altitude control, the adaptive parameter $\hat{m}$ in the altitude controller changes significantly during the ascending process. On the one hand, the ascending process is short, while the convergence of the adaptive parameter requires time. On the other hand, wind drag imposed on the vehicle during the ascent will also change the adaptive parameters, and the size of wind drag varies with movement speed. After reaching the desired altitude, the $\hat{m}$ quickly converges to a stable range. We take the output of the TD in the altitude controller as the reference height and obtain that the RMS of the altitude error during the entire flight was 4.29 cm. Even if the random change of the attitude angle causes the thrust change in the vertical direction, the altitude control still maintains high accuracy, which benefits from the reasonable control distribution design. For example, when the flapping plane is tilted for the torque required in the yaw axis, according to the calculation of control distribution, the motor speed will be increased at the same time to make up for the loss of vertical thrust force due to the change of thrust direction, instead of waiting for roll angular error or the altitude error to appear. In the overshoot suppression, the results obtained in the simulation are also verified, both the altitude control and the angle control essentially have no overshoot. In conclusion, even if the thrust on both wings is asymmetrical when the attitude and altitude state are controlled simultaneously, the adaptive controller exhibits better overshoot suppression ability, better decoupling performance, and higher control accuracy.

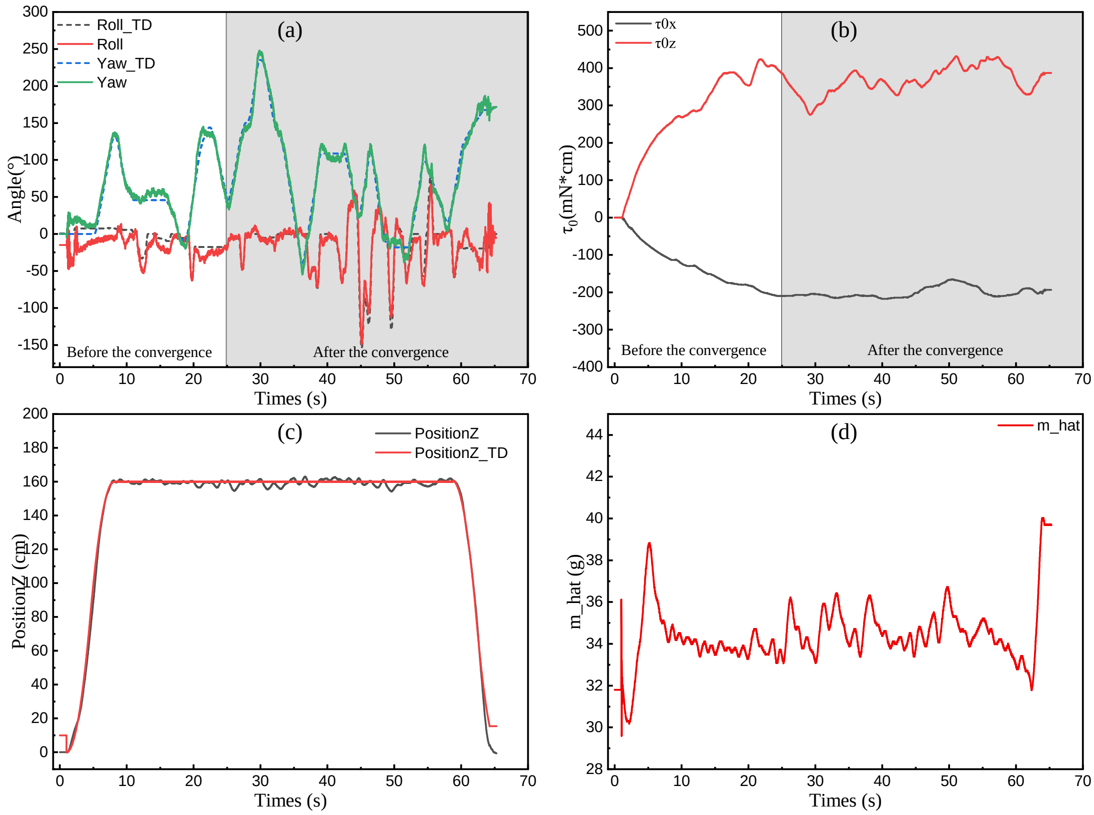

Figure 9. Flight results of the adaptive attitude and altitude controller. The dashed lines are the control references. (**a**) Flight results of attitude control. (**b**) The adaptation of bias torque estimators. (**c**) Flight results of altitude control. (**d**) The adaptation of mass estimator.

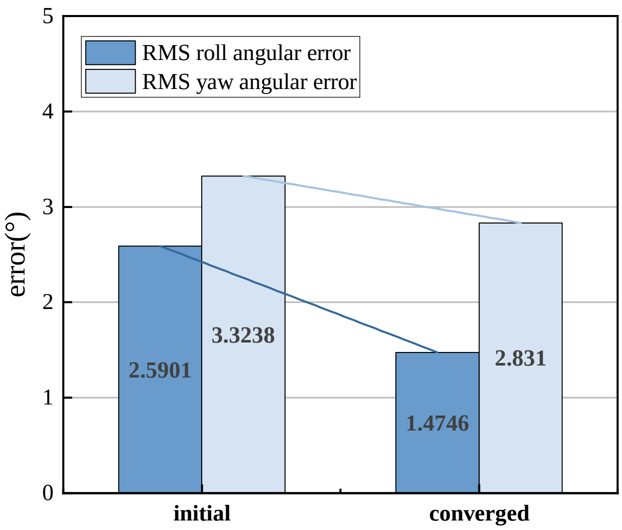

Figure 10. Comparison of RMS angular error before and after adaptive parameter convergence.

5. Conclusions

In this paper, we have introduced the design of a tailless FMAV with a weight of less than 30 g, which can achieve attitude and altitude control using the onboard sensors. Meanwhile, we have established the rotational and translational model of the FMAV. Based on these models, a reasonable control allocation is derived. Compared with the linear combination of the output of each axis controller as the actuator control input, the new control allocation takes into account the mutual influence of each actuator, which can better reduce the coupling effect. In addition, aiming at the problem of model parameter changes or unknown model parameters in the process of assembly or flight, we proposed a multiaxial adaptive controller with the TD as the reference generator. Proper reference trajectory planning can well reduce the overshoot of the system, especially suitable for altitude control or the scene where the reference value has the characteristic of sudden change. In addition, the adaptive parameters in the controller will converge to a stable range during the flight. By comparing the RMS state error before and after convergence, we can see that the adaptive controller plays a key role in improving the control accuracy and eliminating the steady-state error. Even in the case of having unknown bias torque and inaccurate model parameters, the attitude and altitude state of the FMAV can track the reference well. The proposed control scheme has been successfully applied to the FMAV and verified by the simulations and flight. The results show that the designed control scheme has better performance in reducing the overshoot, decoupling, and control accuracy compared to the PID controller. The proposed lightweight FMAV design and controller design provides a new idea for designing more robust flapping wing robots in the future.

Author Contributions: Supervision, planning, concept design, and funding acquisition, W.Z.; Writing, editing, design, and experiment, J.M.; Data acquisition, Q.G.; design, fabrication, C.W. All authors have read and agreed to the published version of the manuscript.

Funding: This research was funded by the Ministry of Education of the People's Republic of China, grant no. 6141A02022627.

Institutional Review Board Statement: Not applicable.

Informed Consent Statement: Not applicable.

Data Availability Statement: Not applicable.

Acknowledgments: A special thanks is due to Suncheng Xiang for his valuable suggestion and guidance on the paper writing.

Conflicts of Interest: The funders had no role in the design of the study; in the collection, analyses, or interpretation of data; in the writing of the manuscript, or in the decision to publish the results.

Abbreviations

The following abbreviations are used in this manuscript:

FMAV	Flapping-wing Micro Aerial Vehicle
DARPA	Defense Advanced Research Projects Agency
ADRC	Active Disturbance Rejection Controller
TD	Tracking Differential
PCB	Printed Circuit Board
CoM	Center of Mass
CoP	Center of Pressure
RMS	Root-Mean-Square

References

1. Ellington, C.P.; Van Den Berg, C.; Willmott, A.P.; Thomas, A.L. Leading-edge vortices in insect flight. *Nature* **1996**, *384*, 626–630. [CrossRef]
2. Dickinson, M.H.; Lehmann, F.O.; Sane, S.P. Wing rotation and the aerodynamic basis of insect flight. *Science* **1999**, *284*, 1954–1960. [CrossRef] [PubMed]
3. Cravero, C.; Marsano, D. Computational Investigation of the Aerodynamics of a Wheel Installed on a Race Car with a Multi-Element Front Wing. *Fluids* **2022**, *7*, 182. [CrossRef]
4. Fernandez-Gamiz, U.; Gomez-Mármol, M.; Chacón-Rebollo, T. Computational modeling of gurney flaps and microtabs by POD method. *Energies* **2018**, *11*, 2091. [CrossRef]
5. Keennon, M.; Klingebiel, K.; Won, H. Development of the nano hummingbird: A tailless flapping wing micro air vehicle. In Proceedings of the 50th AIAA Aerospace Sciences Meeting Including the New Horizons Forum and Aerospace Exposition, Nashville, TN, USA, 9–12 January 2012; p. 588.
6. Roshanbin, A.; Altartouri, H.; Karásek, M.; Preumont, A. COLIBRI: A hovering flapping twin-wing robot. *Int. J. Micro Air Veh.* **2017**, *9*, 270–282. [CrossRef]

7. Phan, H.V.; Kang, T.; Park, H.C. Design and stable flight of a 21 g insect-like tailless flapping wing micro air vehicle with angular rates feedback control. *Bioinspir. Biomimetics* **2017**, *12*, 036006. [CrossRef]
8. Phan, H.V.; Park, H.C. Mechanisms of collision recovery in flying beetles and flapping-wing robots. *Science* **2020**, *370*, 1214–1219. [CrossRef]
9. Phan, H.V.; Park, H.C. Generation of control moments in an insect-like tailless flapping-wing micro air vehicle by changing the stroke-plane angle. *J. Bionic Eng.* **2016**, *13*, 449–457. [CrossRef]
10. Phan, H.V.; Aurecianus, S.; Kang, T.; Park, H.C. KUBeetle-S: An insect-like, tailless, hover-capable robot that can fly with a low-torque control mechanism. *Int. J. Micro Air Veh.* **2019**, *11*, 1756829319861371. [CrossRef]
11. Tu, Z.; Fei, F.; Deng, X. Untethered flight of an at-scale dual-motor hummingbird robot with bio-inspired decoupled wings. *IEEE Robot. Autom. Lett.* **2020**, *5*, 4194–4201. [CrossRef]
12. Tu, Z.; Fei, F.; Zhang, J.; Deng, X. An at-scale tailless flapping-wing hummingbird robot. I. Design, optimization, and experimental validation. *IEEE Trans. Robot.* **2020**, *36*, 1511–1525. [CrossRef]
13. Zhang, J.; Fei, F.; Tu, Z.; Deng, X. Design optimization and system integration of robotic hummingbird. In Proceedings of the 2017 IEEE International Conference on Robotics and Automation (ICRA), Singapore, 29 May–3 June 2017; pp. 5422–5428.
14. Zhang, J.; Tu, Z.; Fei, F.; Deng, X. Geometric flight control of a hovering robotic hummingbird. In Proceedings of the 2017 IEEE International Conference on Robotics and Automation (ICRA), Singapore, 29 May–3 June 2017; pp. 5415–5421.
15. Ma, K.Y.; Chirarattananon, P.; Fuller, S.B.; Wood, R.J. Controlled flight of a biologically inspired, insect-scale robot. *Science* **2013**, *340*, 603–607. [CrossRef] [PubMed]
16. Karásek, M.; Koopmans, A.J.; Armanini, S.F.; Remes, B.D.; de Croon, G.C. Free flight force estimation of a 23.5 g flapping wing MAV using an on-board IMU. In Proceedings of the 2016 IEEE/RSJ International Conference on Intelligent Robots and Systems (IROS), Daejeon, Korea, 9–14 October 2016; pp. 4963–4969.
17. Karásek, M.; Muijres, F.T.; De Wagter, C.; Remes, B.D.; De Croon, G.C. A tailless aerial robotic flapper reveals that flies use torque coupling in rapid banked turns. *Science* **2018**, *361*, 1089–1094. [CrossRef] [PubMed]
18. Verboom, J.; Tijmons, S.; De Wagter, C.; Remes, B.; Babuska, R.; de Croon, G.C. Attitude and altitude estimation and control on board a flapping wing micro air vehicle. In Proceedings of the 2015 IEEE International Conference on Robotics and Automation, Seattle, WA, USA, 26–30 May 2015; pp. 5846–5851.
19. Roshanbin, A.; Garone, E.; Preumont, A. Precision Stationary Flight of a Robotic Hummingbird. In Proceedings of the 2019 International Conference on Robotics and Automation (ICRA), Montreal, QC, Canada, 20–24 May 2019; pp. 7741–7747.
20. Karásek, M.; Percin, M.; Cunis, T.; van Oudheusden, B.W.; De Wagter, C.; Remes, B.D.; de Croon, G.C. Accurate position control of a flapping-wing robot enabling free-flight flow visualisation in a wind tunnel. *Int. J. Micro Air Veh.* **2019**, *11*, 1756829319833683. [CrossRef]
21. Aurecianus, S.; Phan, H.V.; Kang, T.; Park, H.C. Longitudinal mode model-based controller design for tailless flapping wing robot with loop shaping compensator. *Bioinspir. Biomimetics* **2020**, *15*, 056004. [CrossRef]
22. Nguyen, Q.V.; Chan, W.L. Development and flight performance of a biologically-inspired tailless flapping-wing micro air vehicle with wing stroke plane modulation. *Bioinspir. Biomimetics* **2018**, *14*, 016015. [CrossRef]
23. Chirarattananon, P.; Ma, K.Y.; Wood, R.J. Adaptive control of a millimeter-scale flapping-wing robot. *Bioinspir. Biomimetics* **2014**, *9*, 025004. [CrossRef]
24. Tu, Z.; Fei, F.; Liu, L.; Zhou, Y.; Deng, X. Flying with damaged wings: The effect on flight capacity and bio-inspired coping strategies of a flapping wing robot. *IEEE Robot. Autom. Lett.* **2021**, *6*, 2114–2121. [CrossRef]
25. Mou, J.; Zhang, W.; Zheng, K.; Wang, Y.; Wu, C. More Detailed Disturbance Measurement and Active Disturbance Rejection Altitude Control for a Flapping Wing Robot Under Internal and External Disturbances. *J. Bionic Eng.* 2022, *online ahead of print*. [CrossRef]
26. Bai, K.; Luo, Y.; Dan, Z.; Zhang, S.; Wang, M.; Qian, Q.; Zhong, J. Extended State Observer based Attitude Control of a Bird-like Flapping-wing Flying Robot. *J. Bionic Eng.* **2020**, *17*, 708–717. [CrossRef]
27. Han, J. From PID to active disturbance rejection control. *IEEE Trans. Ind. Electron.* **2009**, *56*, 900–906. [CrossRef]
28. Gao, Z. Scaling and bandwidth-parameterization based controller tuning. In Proceedings of the 2003 American Control Conference, Denver, CO, USA, 4–6 June 2003; pp. 4989–4996.
29. Jardin, M.; Mueller, E. Optimized measurements of UAV mass moment of inertia with a bifilar pendulum. In Proceedings of the AIAA Guidance, Navigation and Control Conference and Exhibit, Hilton Head, SC, USA, 20–23 August 2007; p. 6822.
30. Zheng, K.; Zhang, W.; Mou, J.; Wu, C.; Wang, Y. A Nonlinear Longitudinal Model and Its Identification of a Tailless Flapping Wing MAV with Stroke Plane Modulation. In *Lecture Notes in Electrical Engineering, Proceedings of the 2021 International Conference on Autonomous Unmanned Systems, Changsha, China, 24–26 September 2021*; Springer: Singapore, 2021; pp. 2165–2176.
31. Kajak, K.M.; Karásek, M.; Chu, Q.P.; De Croon, G. A minimal longitudinal dynamic model of a tailless flapping wing robot for control design. *Bioinspir. Biomimetics* **2019**, *14*, 046008. [CrossRef] [PubMed]